Nanoscale Research Letters
a SpringerOpen Journal

NANO EXPRESS Open Access

Preparation and characterization of spindle-like Fe_3O_4 mesoporous nanoparticles

Shaofeng Zhang[1,2], Wei Wu[1,2], Xiangheng Xiao[1,2], Juan Zhou[1,2], Feng Ren[1,2*], Changzhong Jiang[1,2*]

Abstract

Magnetic spindle-like Fe_3O_4 mesoporous nanoparticles with a length of 200 nm and diameter of 60 nm were successfully synthesized by reducing the spindle-like α-Fe_2O_3 NPs which were prepared by forced hydrolysis method. The obtained samples were characterized by transmission electron microscopy, powder X-ray diffraction, attenuated total reflection fourier transform infrared spectroscopy, field emission scanning electron microscopy, vibrating sample magnetometer, and nitrogen adsorption-desorption analysis techniques. The results show that α-Fe_2O_3 phase transformed into Fe_3O_4 phase after annealing in hydrogen atmosphere at 350°C. The as-prepared spindle-like Fe_3O_4 mesoporous NPs possess high Brunauer-Emmett-Teller (BET) surface area up to ca. 7.9 m^2 g^{-1}. In addition, the Fe_3O_4 NPs present higher saturation magnetization (85.2 emu g^{-1}) and excellent magnetic response behaviors, which have great potential applications in magnetic separation technology.

Introduction

In the past few decades, porous materials have been used in many fields, such as filters, catalysts, cells, supports, optical materials, and so on [1-3]. In general, porous materials can be classified into three types depending on their pore diameters, namely, microporous (<2 nm), meso- or transitional porous (2-50 nm), and macroporous (>50 nm) materials, respectively [4]. Currently, the mesoporous materials have attracted growing research interests and have great impact in the applications of catalysis, separation, adsorption and sensing due to their special structural features such as special surface area and interior void [2,5-8]. On the other hand, iron oxide nanomaterials have been extensively studied by material researchers in recent years, due to their novel physicochemical properties and advantages (high saturation magnetization, easy synthesis, low cost, etc.) and wide applications in many fields (magnetic recording, pigment, magnetic separation, and magnetic resonance imaging, MRI) [9-16].

However, it is crucial to realize the magnetic iron oxide materials with mesoporous structure which can further adjust the physical and chemical properties of iron oxides for expanding application. According to the previous studies, the porous iron oxide nanomaterials have remarkable magnetic properties, special structures and greatly potential applications in targetable or recyclable carriers, catalyst and biotechnology [17,18]. For example, Yu et al. [19] fabricated novel cage-like Fe_2O_3 hollow spheres on a large scale by hydrothermal method. In the report carbonaceous polysaccharide spheres were used as templates, and the prepared Fe_2O_3 hollow spheres exhibit excellent photocatalytic activity for the degradation of rhodamine B aqueous solution under visible-light illumination. Wu et al. [20] successfully developed porous iron oxide-based nanorods used as nanocapsules for drug delivery, and this porous magnetic nanomaterial exhibited excellent biocompatibility and controllability for drug release.

It is well known that the intrinsic properties of an iron oxide nanomaterial are mainly determined by its size, shape, and structure. A key problem of synthetically controlling the shape and structure of iron oxide nanomaterials has been intensively concerned by many researchers. In previous studies, there have been various porous iron oxide nanomaterials, such as porous α-Fe_2O_3 nanorods, Fe_3O_4 nanocages, and so on [9,21-25]. However, to our best knowledge, there are few reports for fabricating the mesoporous structure of monodisperse spindle-like Fe_3O_4 NPs. Thus, we employ forced hydrolysis method to prepare spindle-like α-Fe_2O_3 NPs first. Then as-prepared α-Fe_2O_3 NPs were reduced by

* Correspondence: fren@whu.edu.cn; czjiang@whu.edu.cn
[1]Key Laboratory of Artificial Micro- and Nano-structures of Ministry of Education, Wuhan University, Wuhan 430072, P. R. China
Full list of author information is available at the end of the article

hydrogen gas at different temperatures. The structure, morphology, and magnetic properties of samples were investigated by multiple analytical technologies. The results reveal that spindle-like Fe_3O_4 mesoporous NPs could be obtained after annealing at 350°C.

Experimental section

Materials

Ferric chloride hexahydrate ($FeCl_3{\cdot}6H_2O$) was purchased from Tianjin Kermel Chemical Reagent CO., Ltd. (Tianjin, China), ethanol (C_2H_5OH, 95% (v/v)) and sodium dihydrogen phosphate dihydrate (NaH_2PO_4) were purchased from Sinopharm Chemical Reagent Co., Ltd. (Shanghai, China), and all regents used were analytically pure (AR) and as received without further purification. The used water was double distilled water.

Synthesis of α-Fe_2O_3 and Fe_3O_4 NPs

Forced hydrolysis method is normally used for the synthesis of α-Fe_2O_3 NPs [26]. In the typical procedure, $NaH_2PO_4{\cdot}2H_2O$ (0.0070 g) was dissolved into 100 ml of water. After completely dissolving, the solution was transferred to a flask (100 ml) and heated to 95°C. Then 1.8 ml of $FeCl_3$ solution (1.48 mol l^{-1}) was added dropwise into the flask, and the mixture was aged at 100°C for 14 h. After the resulting mixture was cooled down to room temperature naturally, the product was centrifuged and washed with double distilled water and ethanol. The as-obtained α-Fe_2O_3 NPs was labeled as S1. The dried α-Fe_2O_3 powder was annealed at 250, 300, 350, 400, and 450°C in hydrogen atmosphere for 5 h. These annealed powders were labeled as S2, S3, S4, S5, S6, respectively. All the samples were dispersed into ethanol solution.

Characterization

XRD patterns of the samples were obtained by using an X'Pert PRO X-ray diffractometer with Cu Kα radiation (λ = 0.154 nm) at a rate of 0.002° 2θ s^{-1}, which was operated at 40 kV and 40 mA. TEM images and selected area electron diffraction (SAED) patterns were performed by a JEOL JEM-2010 (HT) transmission electron microscope operated at 200 kV, the samples were dissolved in ethanol and dropped directly onto the carbon-covered copper grids. SEM analysis of the samples was carried out with a FEI SIRION FESEM operated at an acceleration voltage of 25 kV. The BET surface area of the sample was measured by nitrogen adsorption in a Micromeritics ASAP 2020 nitrogen adsorption apparatus. The samples were degassed before the measurement. Magnetic hysteresis loops of samples were performed in Quantum Design PPMS (Physical Property Measurement System) equipped with a vibrating sample magnetometer (VSM) at room temperature with the external field up to 15 kOe. ATR-FTIR spectra were performed on a Thermo Fisher Nicolet iS10 FT-IR.

Results and discussion

Forced hydrolysis method has been widely used for preparing α-Fe_2O_3 NPs since the first study by Matijevic et al. [4] and Cornell and Schwertmann [27]. In general, in the presence of water, the Fe^{3+} salt dissociates to form the purple, hexa-aquo ion, the electropositive cations induce the H_2O ligands to act as acids (except at very low PH) and hydrolysis by heating. In addition, the Fe salt was added to preheated water in order to avoid nucleation of geothite during the initial heating stage [4,28]. The synthesis of Fe_3O_4 NPs can be reached by reduction of α-Fe_2O_3 NPs in hydrogen atmosphere. In brief, the whole experimental process can be described as follows [4]:

$$FeCl_3 + 6H_2O \rightarrow Fe\left(H_2O\right)_6^{3+} + 3Cl^- \quad (1)$$

$$2Fe\left(H_2O\right)_6^{3+} \rightarrow Fe_2O_3 + 6H^+ + 9H_2O \quad (2)$$

$$3Fe_2O_3 + H_2 \rightarrow 2Fe_3O_4 + H_2O \quad (3)$$

In the hydrolysis process, the features that affect the products of the experiment generally include additive, reaction temperature, aging time, PH value. On the basis of previous reports, the addition anions have great effect on the shape of α-Fe_2O_3 NPs. The used PO_4^{3-} anions will adsorb onto the crystal planes parallel to the *c*-axis of α-Fe_2O_3, which causes the growing of the α-Fe_2O_3 NPs along the c-axis direction and promotes the formation of spindle-like α-Fe_2O_3 NPs [22,29,30]. More detailed formation mechanisms in this study are currently under way.

Figure 1 shows the XRD patterns of the samples. Curve a is the pattern of S1. The diffraction peaks (2θ = 24.1°, 33.2°, 35.6°, 40.9°, 49.5°, 54.1°, 62.4°, and 64.1°) are coincided well with the value of JCPDS card 33-0664 (shown as green lines in the bottom), which could be well indexed to the pure hexagonal phase of hematite ((012), (104), (110), (113), (024), (116), (214), and (300)). Curve b displays the diffraction peaks of S2 (250°C). In this curve all the peak positions do not change, which reveals that the sample is still in α-Fe_2O_3 phase after annealing at this temperature. However, when the annealing temperature elevates to 300°C (S3), some new peaks (2θ = 30.2°, 43.3°, 57.3°, and 62.8°) are appeared in curve c. These peaks can be indexed to cubic spinel magnetite (JCPDS card 19-0629, indexed with red lines in the bottom). Moreover, the peaks of α-Fe_2O_3 become weak, which implies that the α-Fe_2O_3 NPs partially

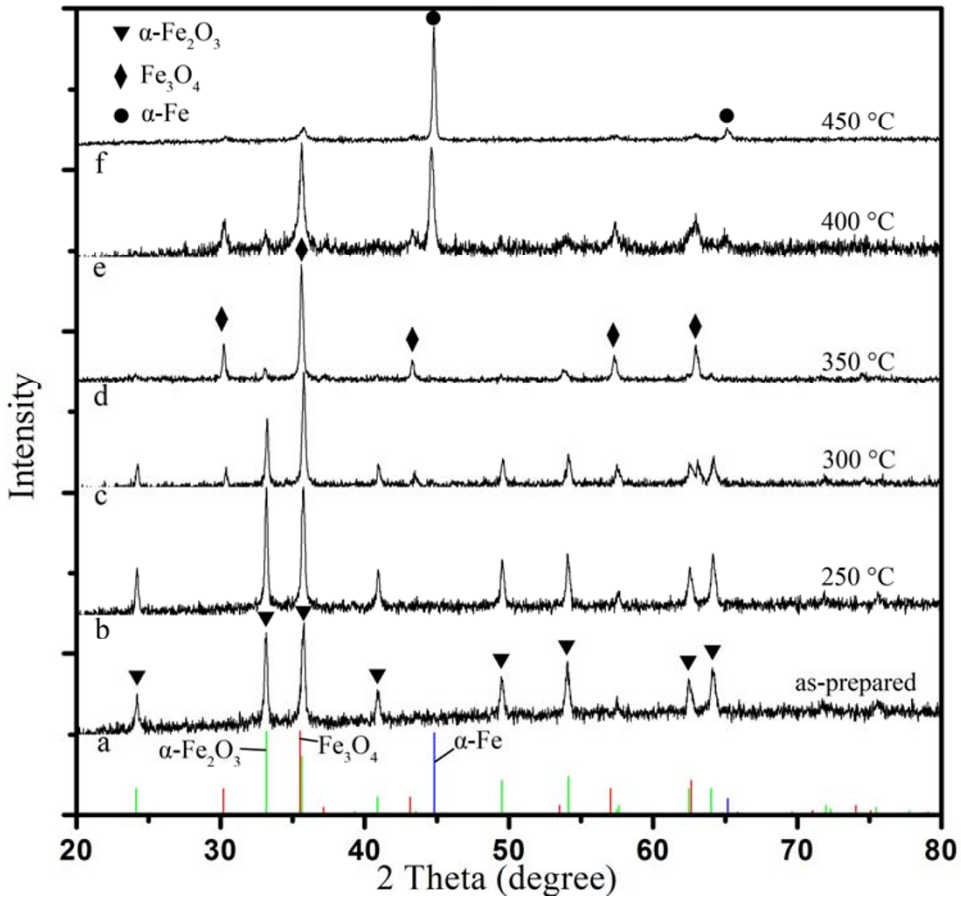

Figure 1 XRD patterns of the samples S1 (a), S2 (b), S3 (c), S4 (d), S5 (e), and S6 (f).

transform to Fe_3O_4 NPs after annealing at 300°C. Subsequently, all the peaks in the pattern of S4 (350°C) could be attributed to Fe_3O_4, their intensity become much stronger. The peaks attribute to α-Fe_2O_3 are almost disappeared, which demonstrates that the NPs is mainly Fe_3O_4 NPs. When the temperature was increased to 400°C (S5, shown in curve e), the peaks (2θ = 44.7°, and 65.0°) can be attributed to α-Fe (JCPDS card 06-0696, shown as blue lines in the bottom). Finally, the sample of S6 mainly transforms to α-Fe phase after annealing at 450°C (curve f).

The morphologies of the samples were studied by SEM analysis. The SEM image of S1 in Figure 2a clearly shows the formation of uniform spindle-like α-Fe_2O_3 NPs with the length and outer diameter approximately 250 and 60 nm, respectively. It is obvious that each of the spindle-like particles possesses a rough surface composed of many small particles. Figure 2b,c,d,e,f shows the SEM images of S2, S3, S4, S5, and S6, respectively. In the Figure 2b,c,d, their particle shape and size are preserved well. However, as shown in Figure 2e, when the annealing temperature increases to 400°C, the shape of the particles is damaged and many particles are melted. For the sample annealed at 450°C (shown in Figure 2f), the spindle-shape of precursor α-Fe_2O_3 NPs is disappeared completely. Instead, the obtained particles have irregular morphology. All the XRD and SEM results clearly indicate that α-Fe_2O_3 NPs can be transformed to Fe_3O_4 NPs after annealing in the reducing atmosphere with temperature up to 350°C, meanwhile the shape and size of the NPs are kept.

For further discussing the morphologies and structures of the samples, TEM images of S1, S2, S4, and S5 are presented, as shown in Figure 3. It can be found in Figure 3a that the as-prepared α-Fe_2O_3 NPs are consisted of smaller closely packed particles, which causes rough surfaces. The inserted SAED pattern is in agreement with the structure plane of α-Fe_2O_3, which also reveals that the α-Fe_2O_3 NPs are in polycrystal. The TEM image of S2 in Figure 2b clearly illustrates that the NPs are mesoporous structure. The SAED pattern demonstrates that the sample is also in polycrystal feature with α-Fe_2O_3 phase. The results reveal that the porous structure has been formed after annealing at

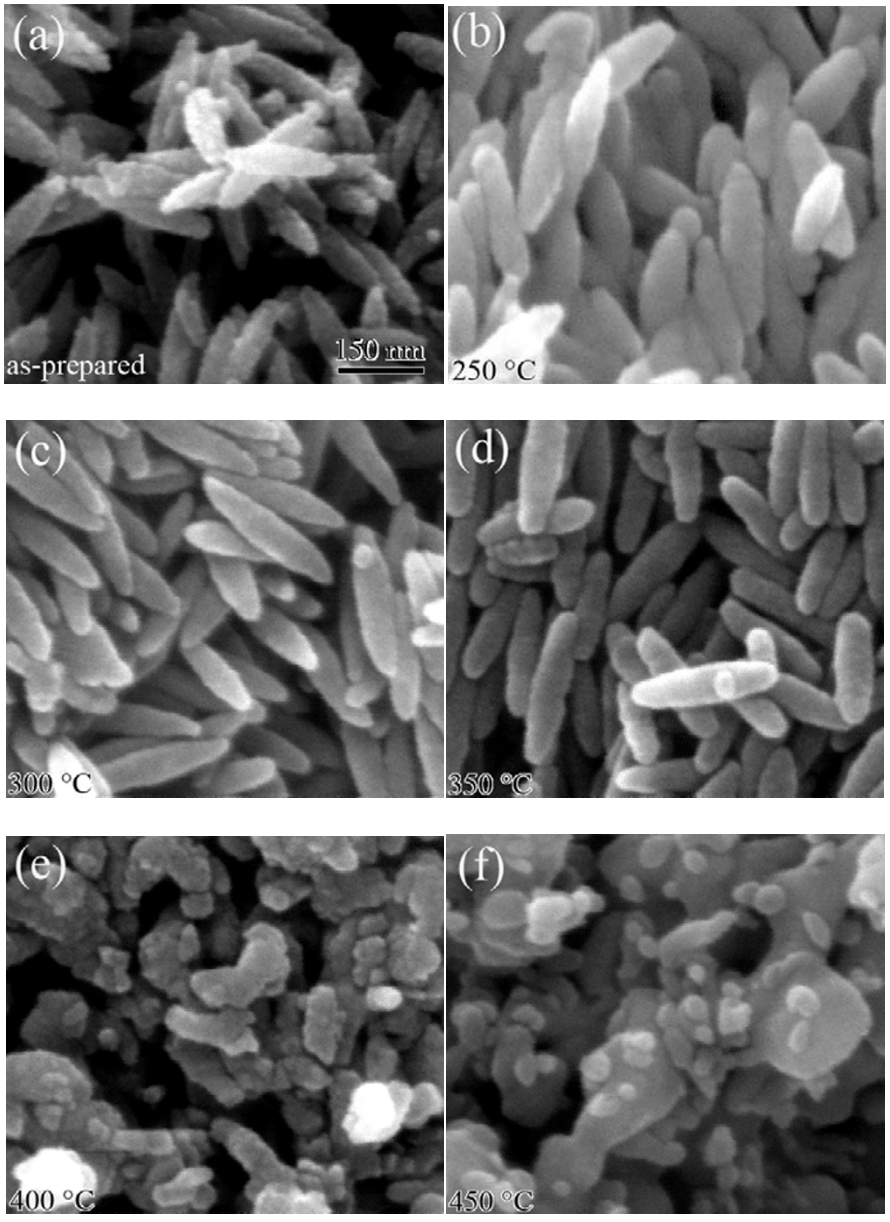

Figure 2 SEM images of the samples S1 (a), S2 (b), S3 (c), S4 (d), S5 (e), and S6 (f).

250°C. Figure 3c shows the TEM image of S3 annealed at 300°C. It can be clearly seen that the shape and size of the particles are well preserved. Moreover, the size of the pores in the sample becomes larger than that of the pores in S2. This is because more vacancies are produced after reducing by H_2. These vacancies aggregate to form larger pores. The inserted SAED pattern implied that the sample S3 is a compound of Fe_3O_4 and α-Fe_2O_3, which coincides with the XRD result. Figure 3d displays the TEM images of S4 (350°C). Although the sample S3 and S4 have similar porous structure, the SAED patterns of the samples are changed and the ring patterns of S4 can be indexed as a cubic spinel phase of magnetite, which demonstrates that the sample S4 are in Fe_3O_4 phase. Figure 3e shows the TEM images of S5. Clearly, some particles are also spindle-like and porous in structure. However, most of the particles are irregularly shaped, meaning that the shape of the sample has been partly damaged after annealing temperature at 400°C. This may be due to the collapse of NP structure, which is because too many large pores are produced inside the NP. The inserted SAED patterns reveal that the sample is a compound of Fe_3O_4 and α-Fe. The TEM result is in good agreement with the XRD and

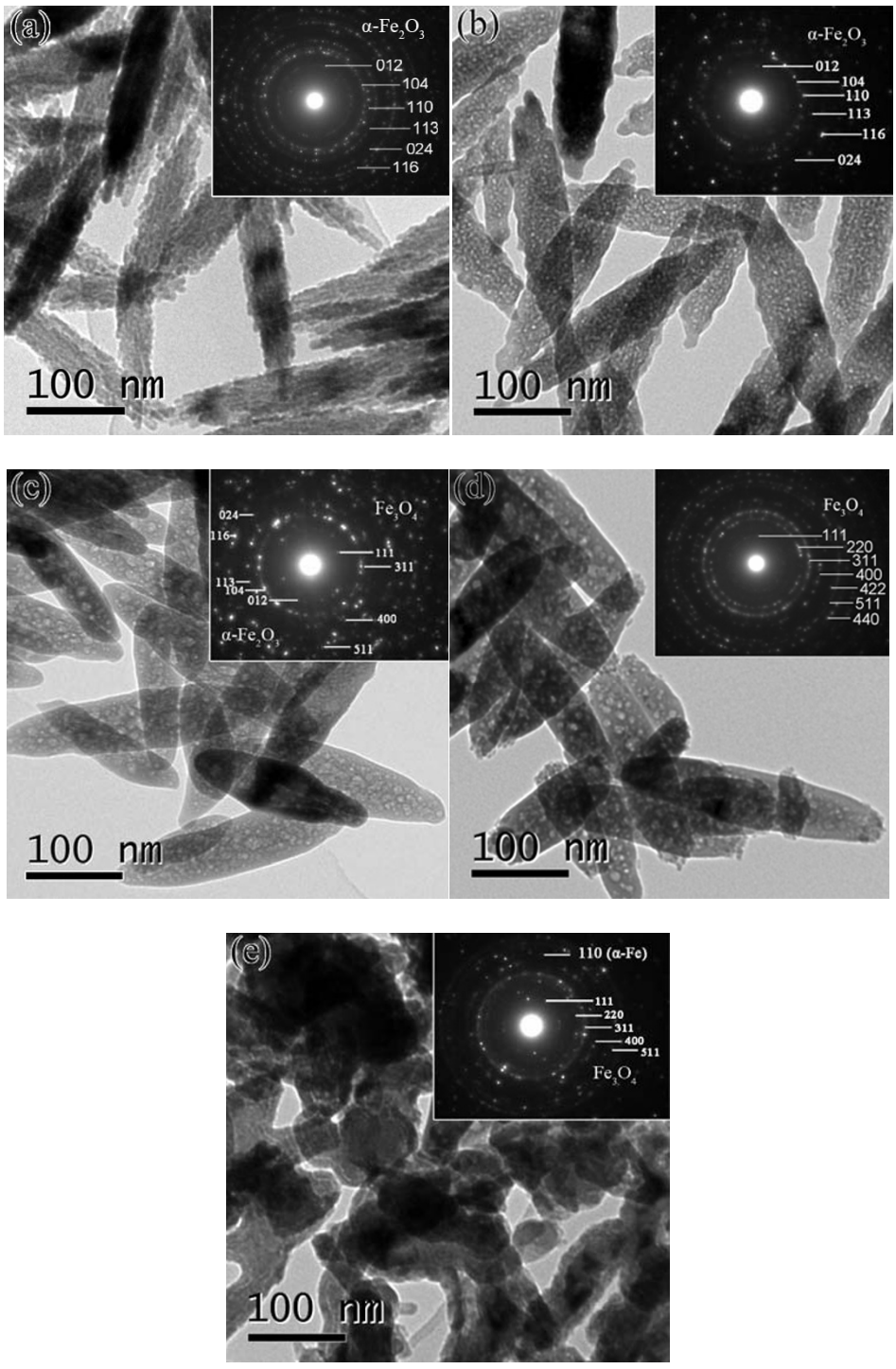

Figure 3 TEM images and corresponding SAED patterns of samples S1 (a), S2 (b), S3 (c), S4 (d), and S5 (e).

SEM results. Moreover, it proves that the annealing treatment can cause the mesoporous structure.

Figure 4 shows the ATR-FTIR spectra of the samples S1 (a) and S4 (b). The absorption band at 558.86 cm^{-1} in the curve a is attributed to the bending vibrations of the Fe-O in α-Fe_2O_3 [31], while the fingerprint bands at 1037.89, 1004.85, 967.99, and 928.40 cm^{-1} could be related to PO_4^{3-} anions [32]. In the curve b, there is an absorption band at 971.16 cm^{-1}. This band is attributed to $NaFePO_4$ [33], which indicates that a new component

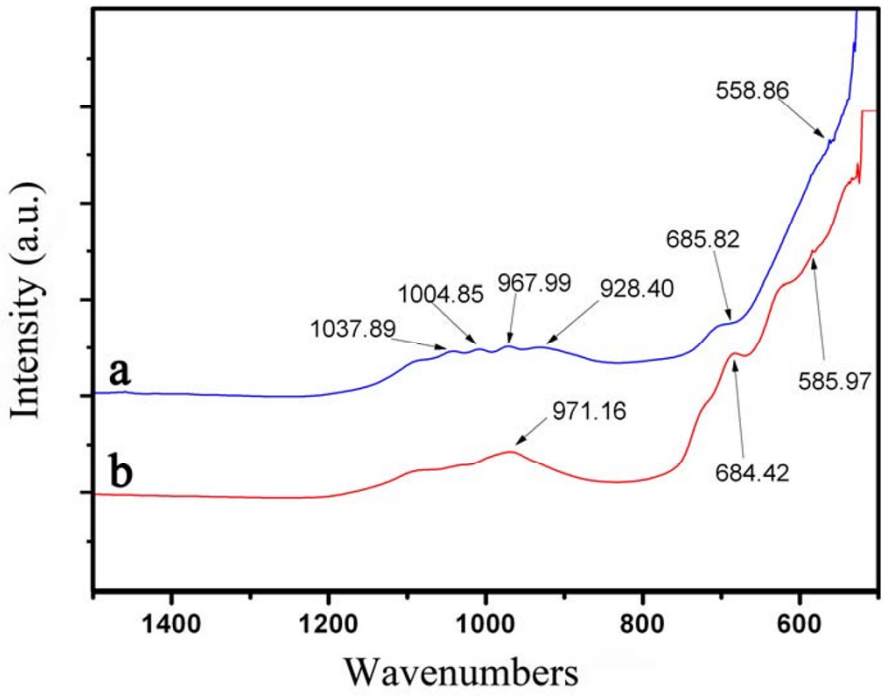

Figure 4 ATR-FTIR spectra of α-Fe_2O_3 NPs (a) and Fe_3O_4 NPs (b).

($NaFePO_4$) might be generated on the surface of the particles after annealing. The absorbtion band at 585.97 cm^{-1} is associated with the Fe-O stretching mode of the Fe_3O_4 NPs [34-36]. In addition, the absorption band at about 685 cm^{-1} is observed in both of the curves, which is assigned to the bending modes of Fe-O-H [31]. The ATR-FTIR results further prove the phase transformation of NPs from α-Fe_2O_3 to Fe_3O_4. Moreover, the detection of the phosphate reveals that the phosphate possibly plays an important role in the formation of the spindle and porous structures.

Nitrogen adsorption-desorption isotherms were performed to determine the surface area and pore size of S4, which is shown in Figure 5. The BET surface area is measured using multipoint BET method within the relative pressure (P/P_0) range from 0.05 to 0.3. The pore size distribution was determined by the Barret-Joyner-Halender (BJH) method using desorption isotherm. The pore volume and average pore size for the sample were determined according to the nitrogen adsorption volume at the relative pressure (P/P_0) of 0.9956. As shown, the sample exhibits a type H3 hysteresis loop according to Brunauer-Deming-Deming-Teller (BDDT) classification, which indicated the presence of mesopores (2-50 nm) with a cylindrical pore mode [37]. According to the BET method, the specific surface area of the samples is determined to be 7.876 $m^2\ g^{-1}$. The BJH adsorption cumulative volume of pores between 17 and 300 nm is 0.15 $cm^3\ g^{-1}$. However, the BJH adsorption average pore of the sample is 78.1 nm, which is probably because the pores in the particles are hermetic, nitrogen could not be contact with the internal wall of the pores [37]. On the other hand, the aggregation of the Fe_3O_4 NPs will cause many spaces among them, which can also lead to the larger result of the pore size [38,39]. The density of the sample based on the current BET result is calculated to be 2.16 g cm^{-3} (Assuming that each Fe_3O_4 NPs is an ellipsoid, thus $\rho = \frac{M}{V}$, and $M = A_s \cdot S$, where ρ is the density of the sample; M, S and V are the mass, surface area and volume of one Fe_3O_4 particle, respectively; A_s is the BET surface area of the sample. As $V = \frac{4}{3}\pi r_a r_b^2$ and $S = 2\pi r_b\left(\frac{7}{3}r_a^2 + \frac{2}{3}r_a r_b + r_b^2\right)$, where r_a and r_b are the length and outer diameter of the Fe_3O_4 NPs, the density of the sample based on the BET result is estimated to be 2.16 g cm^{-3}), it is smaller than 5.18 g cm^{-3} for corresponding bulk Fe_3O_4, which indirectly proves that the Fe_3O_4 NPs are in porous.

As the physicochemical properties of samples are related to their morphologies and structures, the magnetic hysteresis loops of the samples (S1 and S4) were measured by VSM at room temperature, and the results are shown in Figure 6a. From the curve 1, we can see

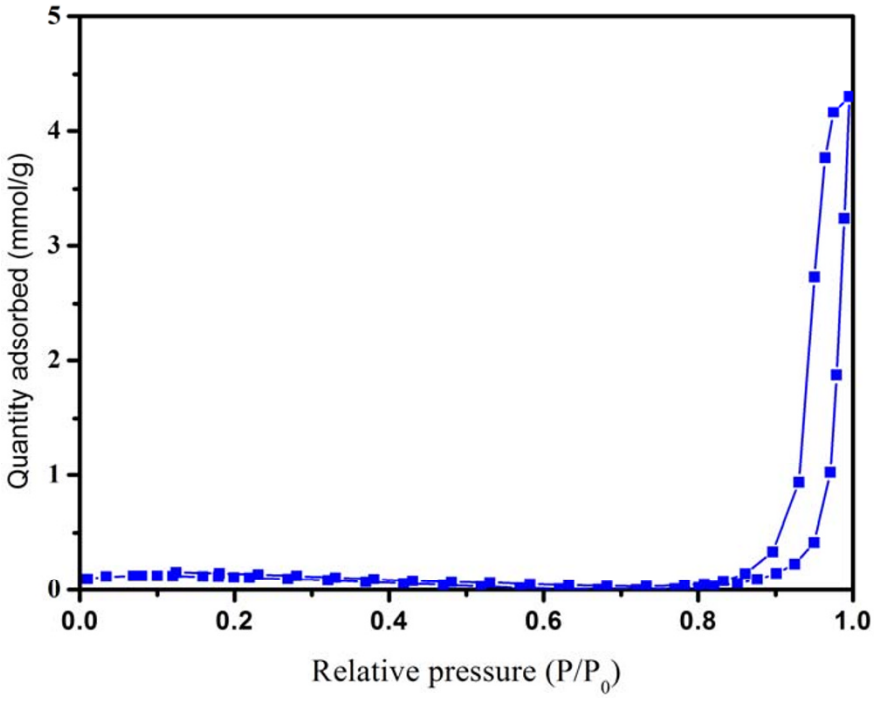

Figure 5 N_2 adsorption and desorption isotherms of Fe_3O_4 NPs.

that the sample exhibits weak ferromagnetic behavior before annealing, and its saturation magnetization and coercivity are 0.64 emu g^{-1} and 37.6 Oe, respectively. It has been proved that the structure of α-Fe_2O_3 can be described as consisting *hcp* arrays of oxygen ions stacked along the [001] direction. Two-thirds of the sites are filled with Fe^{3+} ions, which are arranged regularly with two filled sites being followed by one vacant site in the (001) plane thereby forming sixfold rings. In this case, the arrangement of cations produces pairs of

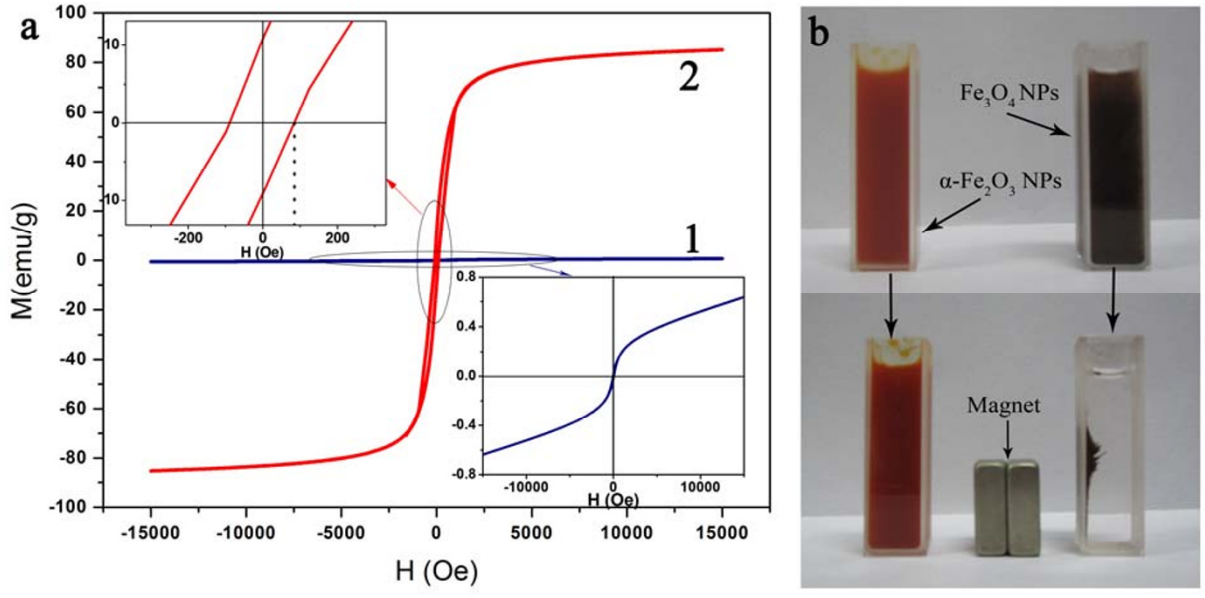

Figure 6 Magnetic hysteresis loops of α-Fe_2O_3 NPs (curve 1) and Fe_3O_4 NPs (curve 2) (a); photographs of α-Fe_2O_3 NPs and Fe_3O_4 NPs before and after magnetic separation with an external magnetic field (b).

$Fe(O)_6$ octahedra, and Fe^{3+} ions are antiferromagnetically coupled across the shared octahedral faces along the c-axis. In the basal plane, there are two interpenetrating antiferromagnetic sublattices. As the electron spins of these sublattices are not exactly antiparallel (with a canting angle of <0.1°), a weak ferromagnetic interaction is resulted, and this effect dominates the magnetic behavior at room temperature [4]. As shown in curve 2 (Figure 6a), the S4 possessed a saturation magnetization of 85.18 emu g^{-1} and a coercivity of 86.01 Oe, the saturation magnetization is close to 92 emu g^{-1} for corresponding bulk Fe_3O_4 [40], which is because the α-Fe_2O_3 phase of the NPs has transformed to Fe_3O_4 phase after annealing. The structure of magnetite is inverse spinel, where there is a face-centered cubic unit cell based on 32 O^{2-} ions which are regularly cubic close packed along the [111]. Two different cation sites occupied by Fe^{2+} and Fe^{3+} form two interpenetrating magnetic sublattices. At room temperature the spins on the two sites are antiparallel and the magnitudes of types of spins are unequal, which causes the ferromagnetism of magnetite. In addition, the particle size and crystal morphology affect the coercivity in the order: spheres < cubes < octahedral in line with the increase in the number of magnetic axes along this series of shapes [4]. In addition, anisotropy shape of the particles may also affect the magnetism [41]. Figure 6b shows the photographs of the samples dispersing in ethanol with and without an external magnetic field. It can be clearly seen that the Fe_3O_4 NPs are well dispersed in ethanol before magnetic separation. However, after magnetic separation all Fe_3O_4 NPs are attracted together by magnet. And the separating time only needs 35 s. For comparison, the α-Fe_2O_3 NPs dispersing in ethanol almost do not change before and after magnetic separation. The results demonstrate that the Fe_3O_4 NPs present excellent magnetic separation property and have good potential application for recyclable nanomaterials.

Summary

In conclusion, spindle-like α-Fe_2O_3 NPs were fabricated by forced hydrolysis of $FeCl_3$ in the presence of PO_4^{3-} anions. The as-prepared α-Fe_2O_3 NPs were then reduced in hydrogen at 350°C and transformed into spindle-like Fe_3O_4 NPs with mesoporous structure. The as-obtained mesoporous Fe_3O_4 NPs possess a high BET surface area of 7.876 m^2 g^{-1}. In addition, the obtained Fe_3O_4 NPs possessed a high saturation magnetization of 85.18 emu g^{-1} and a coercivity of 86.01 Oe. Owing to its excellent magnetic separation property and special mesoporous structure, the as-obtained Fe_3O_4 NPs may have a great potential application in the future.

Abbreviations

AP: analytically pure; ATR-FTIR: attenuated total reflection fourier transform infrared spectroscopy; BDDT: Brunauer-Deming-Deming-Teller; BET: Brunauer-Emmett-Teller; BJP: Barret-Joyner-Halender; FSEM: field emission scanning electron microscopy; MRI: magnetic resonance imaging; NPs: nanoparticles; SAED: selected area electron diffraction; TEM: transmission electron microscopy; VSM: vibrating sample magnetometer; XRD: X-ray diffraction.

Acknowledgements

The author thanks the National Basic Research Program of China (973 Program, No. 2009CB939704), National Mega Project on Major Drug Development (2009ZX09301-014-1), the National Nature Science Foundation of China (No. 10905043, 11005082), Young Chenguang Project of Wuhan City (No. 200850731371, 201050231055), and the Fundamental Research Funds for the Central Universities for financial support.

Author details

[1]Key Laboratory of Artificial Micro- and Nano-structures of Ministry of Education, Wuhan University, Wuhan 430072, P. R. China [2]Center for Electron Microscopy and School of Physics and Technology, Wuhan University, Wuhan 430072, P. R. China

Authors' contributions

SZ participated in the materials preparation, data analysis and drafted the manuscript. WW, XX and JZ participated in the sample characterization. FR conceived and co-wrote the paper. CZ participated in its design and coordination. All authors read and approved the final manuscript.

Competing interests

The authors declare that they have no competing interests.

Received: 18 May 2010 Accepted: 17 January 2011
Published: 17 January 2011

References

1. Ishizaki K, Komarneni S, Nanko M: *Porous Materials: Process Technology and Applications* Boston: Chapman & Hall; 1998.
2. Scott B, Wirnsberger G, Stucky G: **Mesoporous and mesostructured materials for optical applications.** *Chem Mater* 2001, **13**:3140.
3. Wu W, He QG, Jiang CZ: **Magnetic Iron Oxide Nanoparticles: Synthesis and Surface Functionalization Strategies.** *Nanoscale Res Lett* 2008, **3**:397.
4. Cornell R, Schwertmann U: *The Iron Oxides: Structure, Properties, Reactions, Occurrences, and Uses* Weinheim: Wiley-VCH; 2003.
5. Liu J, Liu F, Gao K, Wu J, Xue D: **Magnetic Iron Oxide Nanoparticles: Synthesis and Surface Functionalization Strategies.** *J Mater Chem* 2009, **19**:6073.
6. Yuan ZY, Su BL: **Insights into hierarchically meso-macroporous structured materials.** *J Mater Chem* 2006, **16**:663.
7. Marlow F, Khalil ASG, Stempniewicz M: **Circular mesostructures: solids with novel symmetry properties.** *J Mater Chem* 2007, **17**:2168, (2007).
8. Vinu A, Mori T, Ariga K: **New families of mesoporous materials.** *Sci Technol Adv Mater* 2006, **7**:753.
9. Wu W, Xiao XH, Zhang SF, Li H, Zhou XD, Jiang CZ: **One-Pot Reaction and Subsequent Annealing to Synthesis Hollow Spherical Magnetite and Maghemite Nanocages.** *Nanoscale Res Lett* 2009, **4**:926.
10. Faraji M, Yamini Y, Rezaee M, Magnetic Nanoparticles: **Synthesis, Stabilization, Functionalization, Characterization, and Applications.** *J Iran Chem Soc* 2010, **7**:1.
11. Landon P, Ferguson J, Solsona BE, Garcia T, Al-Sayari S, Carley AF, Herzing AA, Kiely CJ, Makkee M, Moulijn JA, Overweg A, Golunski SE, Hutchings GJ: **Selective oxidation of CO in the presence of H-2, H_2O and CO_2 utilising Au/alpha- Fe_2O_3 catalysts for use in fuel cells.** *J Mater Chem* 2006, **16**:199.
12. Wang Y, Wang YM, Cao JL, Kong FH, Xia HJ, Zhang J, Zhu BL, Wang SR, Wu SH: **Low-temperature H_2S sensors based on Ag-doped alpha-Fe_2O_3 nanoparticles.** *Sens Actuatuator B* 2008, **131**:183.
13. Zhong Z, Ho J, Teo J, Shen S, Gedanken A: **Synthesis of porous alpha-Fe_2O_3 nanorods and deposition of very small gold particles in the pores for catalytic oxidation of CO.** *Chem Mater* 2007, **19**:4776.
14. Tromsdorf UI, Bigall NC, Kaul MG, Bruns OT, Nikolic MS, Mollwitz B, Sperling RA, Reimer R, Hohenberg H, Parak WJ, Forster S, Beisiegel U,

Adam G, Weller H: **Size and surface effects on the MRI relaxivity of manganese ferrite nanoparticle contrast agents.** *Nano Lett* 2007, **7**:2422.
15. Wu CZ, Yin P, Zhu X, Ouyang CZ, Xie Y: **Synthesis of hematite (alpha-Fe_2O_3) nanorods: Diameter-size and shape effects on their applications in magnetism, lithium ion battery, and gas sensors.** *J Phys Chem B* 2006, **110**:17806.
16. Landon P, Ferguson J, Solsona BE, Garcia T, Carley AF, Herzing AA, Kiely CJ, Golunski SE, Hutchings GJ: **Selective oxidation of CO in the presence of H-2, H_2O and CO_2 via gold for use in fuel cells.** *Chem Commun* 2005, 3385.
17. Cheng K, Peng S, Xu CJ, Sun SH: **Porous Hollow Fe_3O_4 Nanoparticles for Targeted Delivery and Controlled Release of Cisplatin.** *J Am Chem Soc* 2009, **131**:10637.
18. Zhong LS, Hu JS, Liang HP, Cao AM, Song WG, Wan LJ: **Self-assembled 3D flowerlike iron oxide nanostructures and their application in water treatment.** *Adv Mater* 2006, **18**:2426.
19. Yu JG, Yu XX, Huang BB, Zhang XY, Dai Y: **Hydrothermal Synthesis and Visible-light Photocatalytic Activity of Novel Cage-like Ferric Oxide Hollow Spheres.** *Cryst Growth Des* 2009, **9**:1474.
20. Wu PC, Wang WS, Huang YT, Sheu HS, Lo YW, Tsai TL, Shieh DB, Yeh CS: **Porous iron oxide based nanorods developed as delivery nanocapsules.** *Chem Eur J* 2007, **13**:3878.
21. Pitzschel K, Moreno JMM, Escrig J, Albrecht O, Nielsch K, Bachmann J: **Controlled Introduction of Diameter Modulations in Arrayed Magnetic Iron Oxide Nanotubes.** *ACS Nano* 2009, **3**:3463.
22. Fan HM, You GJ, Li Y, Zheng Z, Tan HR, Shen ZX, Tang SH, Feng YP: **Shape-Controlled Synthesis of Single-Crystalline Fe_2O_3 Hollow Nanocrystals and Their Tunable Optical Properties.** *J Phys Chem C* 2009, **113**:9928.
23. Omi S, Kanetaka A, Shimamori Y, Supsakulchai A, Nagai M, Ma GH: **Magnetite (Fe_3O_4) microcapsules prepared using a glass membrane and solvent removal.** *J Microencapsule* 2001, **18**:749.
24. Mandal S, Muller AHE: **Facile route to the synthesis of porous alpha-Fe_2O_3 nanorods.** *Mater Chem Phys* 2008, **111**:438.
25. Wu W, Xiao XH, Zhang SF, Fan LX, Peng TC, Ren F, Jiang CZ: **Facile Fabrication of Ultrafine Hollow Silica and Magnetic Hollow Silica Nanoparticles by a Dual-Templating Approach.** *Nanoscale Res Lett* 2010, **5**:116.
26. Ishikawa T, Matijevic E: **Formation of monodispersed pure and coated spindle-type iron particles.** *Langmuir* 1988, **4**:26.
27. Matijevic E, Scheiner P: **Ferric hydrous oxide sols[1,2]: III. Preparation of uniform particles by hydrolysis of Fe (III)-chloride,-nitrate, and-perchlorate solutions.** *J Colloid Interface Sci* 1978, **63**:509.
28. Wang W, Howe JY, Gu BH: **Structure and morphology evolution of hematite (alpha-Fe_2O_3) nanoparticles in forced hydrolysis of ferric chloride.** *J Phys Chem C* 2008, **112**:9203.
29. Almeida TP, Fay M, Zhu YQ, Brown PD: **Process Map for the Hydrothermal Synthesis of alpha-Fe_2O_3 Nanorods.** *J Phys Chem C* 2009, **113**:18689.
30. Lv BL, Xu Y, Wu D, Sun YH: **Preparation and magnetic properties of spindle porous iron nanoparticles.** *Mater Res Bull* 2009, **44**:961.
31. Mitra S, Das S, Mandal K, Chaudhuri S: **Synthesis of a alpha-Fe_2O_3 nanocrystal in its different morphological attributes: growth mechanism, optical and magnetic properties.** *Nanotechnology* 2007, **18**:275608.
32. Stuart B, Infrared Spectroscopy: *Fundamentals and Applications* Chichester: Wiley; 2004.
33. Burba CM, Frech R: **Vibrational spectroscopic investigation of structurally-related $LiFePO_4$, $NaFePO_4$, and $FePO_4$ compounds.** *Spectrochim Acta A* 2006, **65**:44.
34. Liu ZL, Wang X, Yao KL, Du GH, Lu QH, Ding ZH, Tao J, Ning Q, Luo XP, Tian DY, Xi D: **Synthesis of magnetite nanoparticles in W/O microemulsion.** *J Mater Sci* 2004, **39**:2633.
35. Chen FH, Gao Q, Ni JZ: **The grafting and release behavior of doxorubincin from Fe_3O_4@SiO_2 core-shell structure nanoparticles via an acid cleaving amide bond: the potential for magnetic targeting drug delivery.** *Nanotechnology* 2008, **19**:165103.
36. Qiu G, Wang Q, Wang C, Lau W, Guo Y: **Polystyrene/Fe_3O_4 magnetic emulsion and nanocomposite prepared by ultrasonically initiated miniemulsion polymerization.** *Ultrason Sonochem* 2007, **14**:55.
37. Sing K, Everett D, Haul R, Moscou L, Pierotti R, Rouquerol J, Siemieniewska T: **Reporting physisorption data for gas/solid systems with special reference to the determination of surface area and porosity.** *Pure Appl Chem* 1985, **57**:603.
38. Wang Q, Chen YF, Yang M, Wu XF, Tian YJ: **Synthesis of Low Agglomerating Spherical α-Fe_2O_3 Nanopowders.** *Key Eng Mater* 2008, **368-372**:1568.
39. Darab JG, Linehan JC, Matson DW: *Energy Fuels* 1994, **8**:1004.
40. Zhu HL, Yang DR, Zhu LM: **Hydrothermal growth and characterization of magnetite (Fe_3O_4) thin films.** *Surf Coat Technol* 2007, **201**:5870.
41. Bharathi S, Nataraj D, Mangalaraj D, Masuda Y, Senthil K, Yong K: **Highly mesoporous α-Fe2O3 nanostructures: preparation, characterization and improved photocatalytic performance towards Rhodamine B (RhB).** *J Phys D* 2010, **43**:015501.

doi:10.1186/1556-276X-6-89
Cite this article as: Zhang *et al.*: Preparation and characterization of spindle-like Fe_3O_4 mesoporous nanoparticles. *Nanoscale Research Letters* 2011 **6**:89.